**The EMBO Journal (2006) 25,** 3762–3773 | © 2006 European Molecular Biology Organization | All Rights Reserved 0261-4189/06
www.embojournal.org

THE EMBO JOURNAL

# A structural basis for $Mg^{2+}$ homeostasis and the CorA translocation cycle

**Jian Payandeh[1,2,*] and Emil F Pai[1,2,3,4,*]**

[1]Department of Medical Biophysics, University of Toronto, Toronto, Ontario, Canada, [2]Division of Cancer Genomics & Proteomics, Ontario Cancer Institute, MaRS Centre, Toronto Medical Discovery Tower, Toronto, Ontario, Canada, [3]Department of Biochemistry, University of Toronto, Ontario, Canada and [4]Department of Molecular & Medical Genetics, University of Toronto, Toronto, Ontario, Canada

**We describe the CorA $Mg^{2+}$ transporter homologue from *Thermotoga maritima* in complex with 12 divalent cations at 3.7 Å resolution. One metal is found near the universally conserved GMN motif, apparently stabilized within the transmembrane region. This portion of the selectivity filter might discriminate between the size and preferred coordination geometry of hydrated substrates. CorA may further achieve specificity by requiring the sequential dehydration of substrates along the length of its ~55 Å long pore. Ten metal sites identified within the cytoplasmic funnel domain are linked to long extensions of the pore helices and regulate the transport status of CorA. We have characterized this region as an intrinsic divalent cation sensor and provide evidence that it functions as a $Mg^{2+}$-specific homeostatic molecular switch. A proteolytic protection assay, biophysical data, and comparison to a soluble domain structure from *Archaeoglobus fulgidus* have revealed the potential reaction coordinate for this diverse family of transport proteins.**

*The EMBO Journal* (2006) **25,** 3762–3773. doi:10.1038/sj.emboj.7601269; Published online 10 August 2006
*Subject Categories*: membranes & transport; structural biology
*Keywords*: magnesium homeostasis and transport; open state model; selectivity filter; translocation cycle; X-ray crystallography

## Introduction

As the most abundant divalent cation within cells, $Mg^{2+}$ enjoys diverse cellular roles. It helps to stabilize ribosomes and cellular membranes, and is indispensable for maintaining genomic stability (Hartwig, 2001). $Mg^{2+}$ has the largest hydrated radius and the smallest ionic radius among the common biological cations, where its high charge density and relative structural rigidity probably reflects its distinct roles in biology. As such, $Mg^{2+}$ transporters may constitute a unique class of integral membrane proteins (Kehres and Maguire, 2002; Maguire and Cowan, 2002). Only recently have mechanisms of $Mg^{2+}$ homeostasis and transport been revealed at the molecular level (Garcia Vescovi *et al*, 1996; Cromie *et al*, 2006; Lunin *et al*, 2006).

CorA represents the primary $Mg^{2+}$ uptake system in most prokaryotes. It is constitutively expressed and functions to transport $Mg^{2+}$ into cells against a concentration gradient. Named for the cobalt-resistant mutants in which it was first identified, CorA can also transport $Co^{2+}$ and $Ni^{2+}$. The influx of $Co^{2+}$ and $Ni^{2+}$ through CorA may occur as leakage, as the concentrations required for transport would lead to toxicity (Kehres and Maguire, 2002). Under certain conditions, the CorA proteins can also mediate $Mg^{2+}$ efflux (Snavely *et al*, 1989; Liu *et al*, 2002; Kolisek *et al*, 2003), although the relevance of this is not understood. The prokaryotic ZntB subfamily actually mediates $Zn^{2+}$ efflux rather than $Mg^{2+}$ influx (Worlock and Smith, 2002). In yeast, the *alr1* family confers $Al^{3+}$ resistance (MacDiarmid and Gardner, 1998) and encodes the major plasma membrane $Mg^{2+}$ uptake system (Liu *et al*, 2002). The related *mrs2* genes are involved in mitochondrial $Mg^{2+}$ uptake in yeast, plants, and mammals (Bui *et al*, 1999; Zsurka *et al*, 2001; Kolisek *et al*, 2003; Knoop *et al*, 2005). The *mrs2* family has been expanded in plants, and *Arabidopsis thaliana* contains at least 10 genes whose products are targeted to different cellular membranes (Li *et al*, 2001; Knoop *et al*, 2005). It appears that some of these systems are capable of transporting additional divalent cations, including $Cu^{2+}$, $Fe^{2+}$, $Mn^{2+}$, and $Zn^{2+}$ (MacDiarmid and Gardner, 1998; Li *et al*, 2001).

The prokaryotic and eukaryotic CorA/Alr1/Mrs2 proteins can often functionally substitute for one another (Bui *et al*, 1999; Li *et al*, 2001; Zsurka *et al*, 2001; Kehres and Maguire, 2002). In fact, recent structural analysis has confirmed that these diverse transport proteins likely share a common structural scaffold (Lunin *et al*, 2006). Although their precise classification as either ion channels or ion transporters remains somewhat ambiguous (Snavely *et al*, 1989; MacDiarmid and Gardner, 1998; Kehres and Maguire, 2002; Liu *et al*, 2002; Kolisek *et al*, 2003; Lunin *et al*, 2006), these proteins seem to utilize the membrane potential to drive $Mg^{2+}$ uptake (Kolisek *et al*, 2003; Froschauer *et al*, 2004). The CorA transporters share a universally conserved GMN motif within their transmembrane region, and most prokaryotic proteins conserve an MPEL sequence in close proximity (Kehres and Maguire, 2002; Knoop *et al*, 2005). Mutations within the GMN motif are known to abolish $Mg^{2+}$ transport; however, naturally occurring variants might be associated with the transport of other divalent cations (Knoop *et al*, 2005). In general, the sequence similarity among CorA orthologues is highest in the C-terminal membrane-spanning domain and lower within the N-terminal soluble region.

We report crystal structures of the full-length CorA homologue from the thermophilic Gram-negative bacterium *Thermotoga maritima* ($TmCorA_{1-351}$) and of a cytoplasmic domain from the thermophilic archaeon *Archaeoglobus fulgidus* ($AfCorA_{1-263}$) at 3.7 and 2.9 Å resolution, respectively.

*Corresponding authors. Division of Cancer Genomics & Proteomics, Ontario Cancer Institute, MaRS Centre, Toronto Medical Discovery Tower, 101 College Street, Toronto, Ontario, Canada M5G 1L7.
Tel.: 416 581 7545; Fax: 416 581 7545;
E-mail: payandeh@uhnres.utoronto.ca or pai@hera.med.utoronto.ca

**Received: 12 May 2006; accepted: 13 July 2006; published online: 10 August 2006**

 

Our data indicate that a metal is stabilized within the transmembrane region and suggests that the CorA selectivity filter might discriminate between the size and preferred coordination geometry of hydrated cations. In addition, 10 metal-binding sites located within the cytoplasmic funnel domain are characterized as a physiologically tuned divalent cation sensor. This reveals a central role for CorA in prokaryotic $Mg^{2+}$ homeostasis. A major conformational change is observed between $AfCorA_{1-263}$ and $TmCorA_{1-351}$, which allows us to propose an open state model and the structural basis for gating and transport in the CorA superfamily.

## Results

### *Overall structure of CorA*

$TmCorA_{1-351}$ presents a funnel-shaped pentameric assembly with approximate five-fold symmetry around a central pore. It stands over 100 Å in height and can be divided into two parts: a large N-terminal cytoplasmic funnel domain and a smaller C-terminal transmembrane (TM) domain (Figure 1A). Following a portion of the main chain without regular secondary structure, the funnel domain has an α/β structure whose core is composed of a seven-stranded mixed β-sheet (β1–β7). The β-sheet is flanked on one side by three short α-helices (α1–α3) and on the other side by one short (α4) and two long α-helices (α5–α6) (Figure 1B). This portion of the funnel domain is connected to α7, the supporting helix of the entire CorA assembly, which extends towards the membrane to form the central pore-lining TM helices (TM1). The five pore-lining helices are flanked by five additional TM helices (TM2, α8). The $TmCorA_{1-351}$ model was refined to a 3.7 Å resolution with $R$ and $R_{free}$ values of 29.5 and 31.6%, respectively. Data collection and refinement statistics are presented in Supplementary Table 1, along with representative portions of the electron density map (Supplementary Figure 1).

### *Membrane and pore boundaries of CorA*

The metal translocation pathway in CorA is surprisingly long, ~55 Å, from Asn314 to Asp277. This exceeds the ~30 Å hydrophobic stretch expected for a membrane bilayer, but is partially reconciled by considering what portion of the TM domain delineates the membrane boundary. Tyr344 and

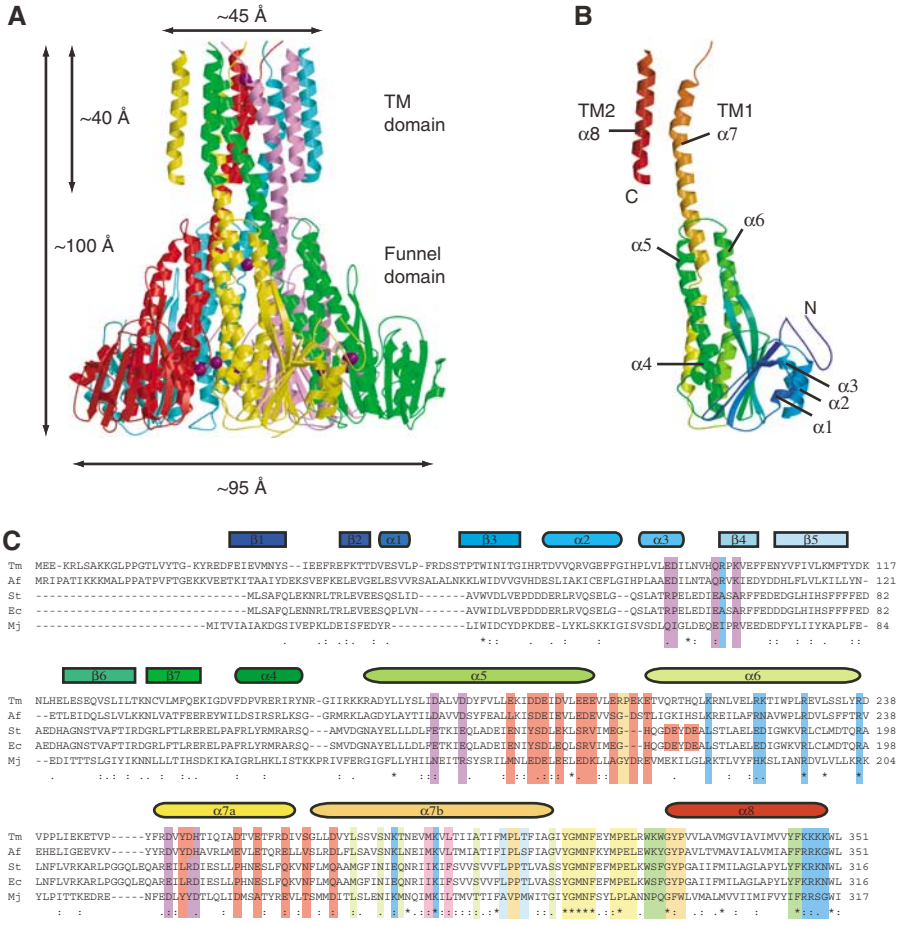


**Figure 1** Structure and sequence alignment of CorA. (**A**) Ribbon diagram of the $TmCorA_{1-351}$ pentamer. Each protomer is colored separately, and purple spheres represent bound $Ca^{2+}$ ions. The funnel domain is cytoplasmic. (**B**) A $TmCorA_{1-351}$ protomer is shaded from blue to red (N- to C-terminus). Helical secondary structural elements are indicated. (**C**) Sequence alignment of prokaryotic CorA proteins from *T. maritima* (Tm), *A. fulgidus* (Af), *S. typhimurium* (St), *E. coli* (Ec), and *M. jannaschii* (Mj). Color coding is as follows: Purple – divalent cation sensor; blue – basic ring (α7b and α8) and funnel domain 'neutralizing residues' (β4 and α6); red – acidic ring (α5 and α6) and funnel domain 'electrostatic sink residues' (α7a and α7b); orange – CorA elbow (α5–α6 loop) and other potential hinges: Pro303 (α7b) and the GYP motif (α8); light green – pore lining residues (α7b); pink – hydrophobic girdle (α7b); light blue – hydrophobic belt (α7b); yellow – GMN motif and MPEL loop; dark green – membrane boundaries (α8). Two potential roles for Asp256 have been indicated. Charge 'switching' can partly account for the overall low sequence identity between CorA homologues.

Phe345 on TM2 create a pronounced aromatic ring at the intracellular lipid–aqueous interface, which aligns with Leu294 on TM1 (Figure 2A and D). The hydrophobic boundary on the periplasmic side of the membrane is more ambiguous (Smith *et al*, 1998; Lunin *et al*, 2006), but probably defined by the well-conserved Trp323-Lys324-Trp325 sequence (Figure 1C). Although this region is difficult to model (see Supplementary Materials and methods), electron density clearly restricts the main chain (Figure 2A), and the side chains of Trp323 and Trp325 should form a prominent aromatic ring at the periplasmic lipid–aqueous interface. A slight lengthening of TM2 allows room to model Glu316–Arg322 within the density observed connecting TM1 to TM2 (Figure 2A). This does not seem possible using a previously determined structure ($TmCorA_{SGC}$; PDB 2BBJ; space group $P2_12_12$), where Trp323–Lys324–Trp325 are modeled in a more extended conformation (Lunin *et al*, 2006).

The membrane boundaries of CorA defined by these two aromatic rings have important consequences. First, the highly conserved MPEL motif (Figure 1C) lies almost parallel with the membrane surface and constitutes the largest portion of the transporter exposed to the periplasmic space (Figure 2A). Second, the universal GMN motif is perpendicular to the plane of the membrane and lines the first portion of the metal translocation pathway (Figure 2A–D). Third, a metal identified within the pore sits ~10 Å into the membrane (Site A;

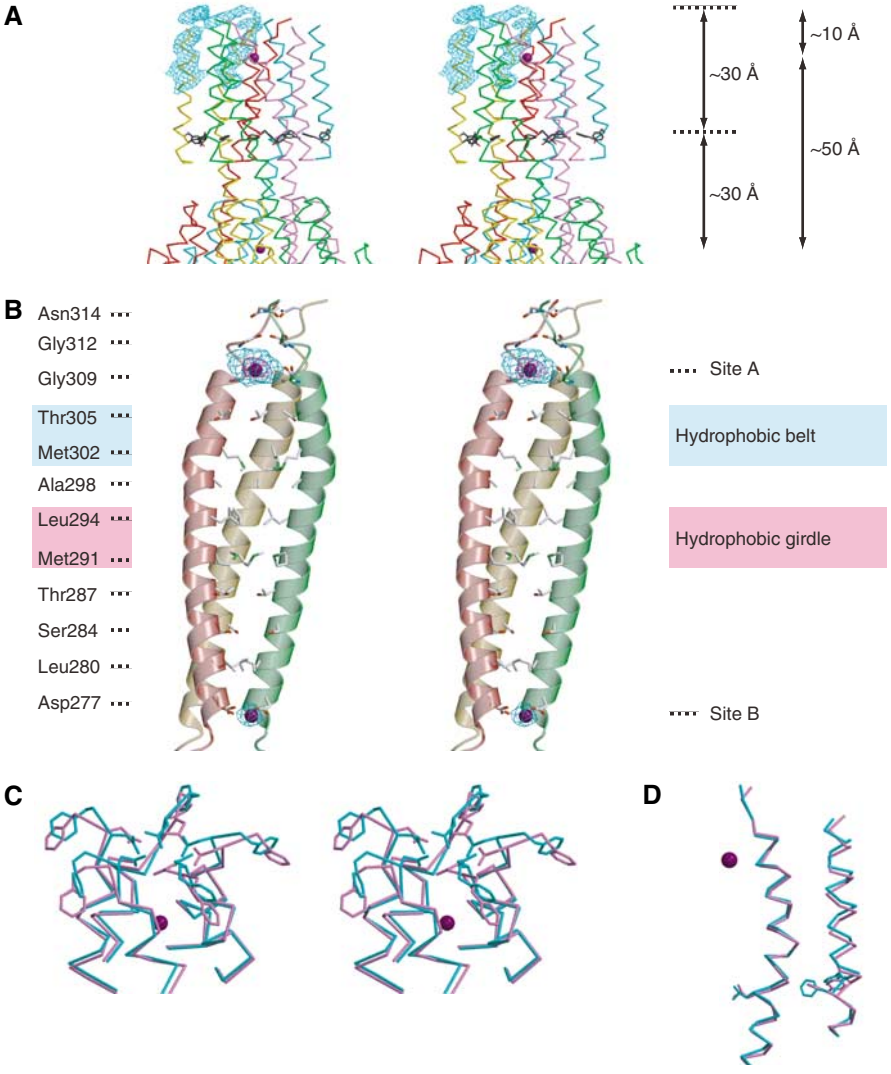


**Figure 2** Membrane and pore boundaries. (**A**) CorA membrane boundaries. In a stereo representation, residues of the intracellular aromatic ring (Tyr344 and Phe345) are shown as stick models. Electron density calculated from a composite omit map contoured at 2σ shows the connectivity between TM1 and TM2 (i.e. the MPEL loop); it also indicates the relative position of the Trp323–Lys324–Trp325 aromatic ring. Purple spheres represent bound $Ca^{2+}$ ions. Approximate distances are indicated. (**B**) Stereo view of the CorA pore. Side chains directed into the pore are shown as stick models; Gly312 and Gly309 are shown in full. Electron density calculated from a composite omit map at Site A indicates the presence of a hydrated cation; blue and purple are contoured at 3σ and 4.5σ, respectively. Electron density at Site B was calculated from a composite omit map and contoured at 3σ (blue). (**C**) Stereo representation of the Asn314 gate. The protein backbone of $TmCorA_{1-351}$ (present work) is colored purple (Site A is included for reference) and $TmCorA_{SGC}$ (PDB 2BBJ) is colored blue. The side chains of Asn314 and Phe315 are shown as stick models. When comparing the two structures, the side chains of Asn314 have moved up to 3 Å. (**D**) One protomer from $TmCorA_{1-351}$ (purple; Site A is included for reference) and $TmCorA_{SGC}$ (blue; Trp323–Lys324–Trp325 have been omitted for clarity) are shown. The side chains of Leu294, Tyr344, and Phe345 are shown as stick models. While both proteins were crystallized under similar conditions and in an apparently closed state, displacements of TM2 >1 Å are observed.

Figure 2A–D). Moreover, a second metal found ~50 Å below Site A is located within the funnel domain; this site marks the intracellular end of the CorA pore (Site B; Figures 1A, 2A and B).

### *The CorA pore*

There are several intriguing features about the CorA pore. For instance, its unprecedented overall length (~55 Å) and its sparingly polar nature. Although the side chains of Asn314 and Asp277 'cap' the pore entrance at either end, only the backbone carbonyls and amides from TM1, the hydroxyls of Thr305, Thr287, and Ser284, and the sulfur atoms from Met302 and Met291 contribute to its polar character (Figure 2B). There are no formal charges and, beyond the GMN motif (Figure 1C), no universally conserved residues line the metal translocation pathway. Another striking feature is the cross-sectional width of the pore; its diameter ranges from ~6 Å near Gly309 and Ala298 to between 3.5 and 2.5 Å at Met302 and Leu294.

The narrowest constriction along the pore occurs at Leu294. This position is highly conserved as a bulky hydrophobic residue in CorA (Figure 1C), and likely serves as the intracellular gate. We refer to this region as the 'hydrophobic girdle', and note that it aligns with the aromatic ring formed by Tyr344-Phe345 (Figure 2A, B and D). We refer to the constriction at Thr305 and Met302 as the 'hydrophobic belt', as it appears to be conserved in the prokaryotic proteins (Figures 1C and 2B). Based on their relative positions within the pore, these features presumably play important roles in determining the substrate specificity of this transporter. As the pore is too narrow for $Mg^{2+}$ to pass while maintaining its first hydration shell (~5 Å), CorA must at least partially dehydrate substrates during transport or achieve a significant dilation of its pore. It is possible that side chain movements might allow for cation transport in the conformation of $TmCorA_{1-351}$ observed in the crystal structure. We note, for example, that the side chains of Asn314 appear to gate the periplasmic pore entrance (Figure 2C; Lunin *et al*, 2006).

### *Metals along the CorA pore*

While final confirmation will require anomalous scattering data, the two metals found along the pore were assigned as calcium ions (Site A and Site B; Figure 2A–C) as $TmCorA_{1-351}$ was crystallized in the presence of 200 mM $CaCl_2$. These sites are separated by a staggering ~50 Å, which is either the closest approach between two cations within the CorA pore, or the closest approach between two bound *calcium* ions under the experimental conditions. As $Ca^{2+}$ is neither a substrate nor a good inhibitor of CorA (Snavely *et al*, 1989), we favor the latter scenario. Moreover, this result would otherwise deviate from the proximal substrate arrangements that are found in other ion channel and ion transporter proteins (Zhou and MacKinnon, 2003; Gouaux and Mackinnon, 2005; Lobet and Dutzler, 2006; Shi *et al*, 2006).

Although the exact coordination sphere cannot be deciphered at the current resolution, the density observed at Site A suggests that a hydrated cation is present (Figure 2B). This would be consistent with the hydrogen-bonding constraints for a hydrated divalent cation, as well as the cross-sectional width of the surrounding pore. Site A also seems reminiscent of the water-hydrated cation found within the central cavity of the KcsA $K^+$ channel (Zhou *et al*, 2001); and movement of the CorA Asn314 side chains may be compatible with the passage of hydrated substrates (Figure 2C). As judged by distance, the Site B metal is likely coordinated through water by the side chains of Asp277 (Figure 2B).

In a previous study, electron density within the pore near Gly309 and Ala298 had suggested the presence of bound ions (Lunin *et al*, 2006). As $TmCorA_{SGC}$ was crystallized in the presence of 300 mM $Mg(NO_3)_2$ (PDB 2BBJ; Lunin *et al*, 2006), it is worth noting that Gly309 is directly adjacent to Site A (Figure 2B). If the cavity near Ala298 can accommodate a hydrated $Mg^{2+}$ ion, as its dimensions suggest, then two hydrated metals may flank the hydrophobic belt at Thr305/Met302 (Figure 2B). Because $Ca^{2+}$ is not a substrate of CorA, and there is no apparent density in the pore near Ala298 within our structure, these comparisons may indicate that the hydrophobic belt performs a critical role in substrate selectivity.

### *CorA electrostatics and the cation sensor*

Many electrostatic surface properties of CorA require mention. TM2 ends with the highly conserved cytoplasmic sequence $KKKKWL_{351}$ (Figure 1C). Therefore, residues Lys346–Lys349 are located near the intracellular lipid–aqueous interface, below the Tyr344–Phe345 aromatic ring (Figure 2A). Together with Lys286 and Lys292 contributed by α7, TmCorA places a total of 30 lysine residues around the pentamer at this membrane proximal region. This 'basic ring' (Figure 3A) may play a role in protein folding (von Heijne, 1989) or as a potential pH sensor (Kloda *et al*, 2006). Although some charge should be neutralized by the surrounding lipid headgroups, this feature will also contribute to the creation of a large dipole. Situated below the basic ring on the funnel domain exterior is an 'acidic ring' (Figure 3A), which is formed by a collection of conserved residues contributed by α5 and α6 (Figure 1C). The relative juxtaposition of these oppositely charged rings could propagate movements onto TM2, the periplasmic MPEL loop, and the GMN motif during the translocation cycle of CorA (Figure 2C and D). Below, we provide evidence demonstrating a conformational plasticity in CorA capable of effecting such an outcome.

Beyond Asp277 of the CorA pore, α7 lines the interior of the funnel domain with acidic and hydroxyl-bearing residues (Figure 1C). This feature could create an electrostatic sink that would help draw $Mg^{2+}$ out of the pore; however, basic residues contributed by α6 and β4 effectively neutralize the desired negative charge character in TmCorA (Figures 1C and 5C). In our open state model (see below), these basic residues are withdrawn and the funnel domain interior becomes extremely acidic (Figure 5D). This could be the key to overcoming the energetic barrier of $Mg^{2+}$ transport through the CorA pore.

The interface between protomers within the funnel domain is also acidic (Figure 5C). As previously suggested (Lunin *et al*, 2006), a cation is coordinated between Asp89′ from α3′ and Asp253 of α7 (′ represents a residue from an adjacent protomer; Figure 3B). A second cation is found coordinated by Asp175 and Asp179 from α5, and probably through waters to Glu88′ of α3′ and His257 from α7 (Figure 3B). A portion of the 'N-terminal flap' (i.e. residues 1–25) closes over this second site and stabilizes it (Figures 3B and 5A). These 10 peripheral metal-binding sites appear to be part of TmCorA's 'divalent cation sensor'. Although Glu88, Asp89, Asp175,

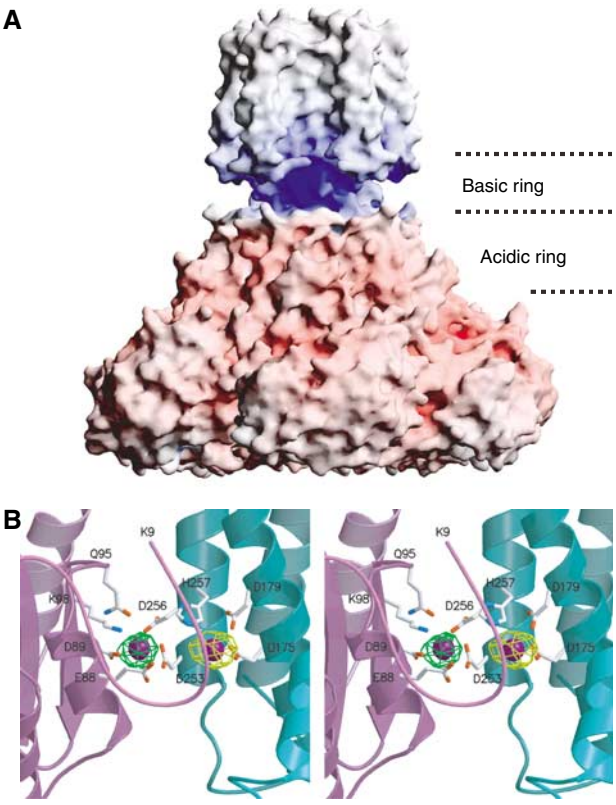


**Figure 3** Charged rings and the divalent cation sensor. (**A**) The electrostatic surface potential of the CorA exterior. Red – acidic regions; blue – basic regions. The view is similar to that in Figure 1A. $Ca^{2+}$ ions were omitted from the calculation. (**B**) Stereo view of residues implicated in the divalent cation sensor and bound $Ca^{2+}$ ions (purple spheres). Electron density calculated from composite omit maps are shown for each site, contoured at 3.5σ. The 'green' metal is coordinated directly by Asp89′ and Asp253. The 'yellow' metal is coordinated by Asp175 and Asp179, and probably through waters to Glu88′ and His257.

Asp179, Asp253, and His257 are highly conserved residues, none are universal (Figure 1C). We anticipate that analogous arrangements exist within all CorA proteins and have indicated some candidate positions (Figures 1C and 3B). Based on the 'minimal' sequences of the well-characterized proteins from *Salmonella typhimurium* (StCorA) and *Methanococcus jannaschii* (MjCorA; Figure 1C), the N-terminal flap interactions may not be essential.

### *Building an open state model*

During efforts to obtain crystallographic phases for $TmCorA_{1-351}$, we crystallized soluble protein constructs from various prokaryotic homologues (Payandeh and Pai, 2006). The structure of $AfCorA_{1-263}$ was solved to 2.9 Å resolution, and a $Co^{2+}$ coordinated to Asp253 and His257 was confirmed experimentally (Figure 4A; see Supplementary Table 1, and Supplementary Materials and methods). It is now apparent that our soluble constructs truncated α7 within the funnel domain. Although the pentameric state is not preserved, and a domain-swapped dimer is observed instead, $AfCorA_{1-263}$ superimposes well with equivalent portions of TmCorA (Figure 4A–C). For instance, the first ~200 residues comprising β1–β7 and α1–α5 are structurally equivalent (RMSD 1.5 Å over 172 $C_\alpha$; Figure 4B and C). Where α5 is the handle, this subdomain resembles a hammer (Figure 4C).

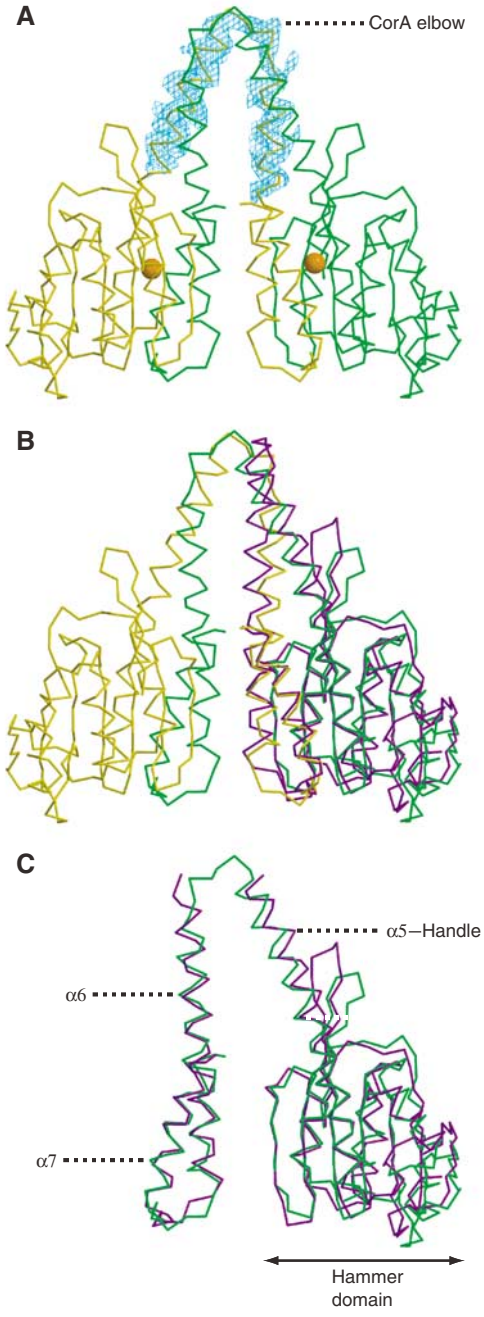


**Figure 4** Structure and comparison of $AfCorA_{1-263}$. (**A**) The 'domain-swapped' molecules of the $AfCorA_{1-263}$ crystal structure are viewed along the screw axis of its $P6_122$ unit cell, where one two-fold axis is perpendicular to the plane of the paper. The orange spheres represent bound $Co^{2+}$ ions coordinated by Asp253 and His257 (these side chains are not shown). A portion of the unbiased experimental electron density from a 3.2 Å Se-MAD experiment is shown over the CorA elbow region of the yellow molecule, contoured at 1.5σ. (**B**) Superposition of the equivalent residues from $TmCorA_{1-351}$ (purple) demonstrates the domain-swapped nature of the $AfCorA_{1-263}$ structure and implicates the CorA elbow as a region of interest. (**C**) Independent alignment of the hammer domains from $AfCorA_{1-263}$ and $TmCorA_{1-351}$ demonstrate their structural likeness, as does the independent superposition of α6 and α7.

Superposition of the hammer domains reveals that α6 and α7 from $AfCorA_{1-263}$ are markedly displaced from their positions in the full-length transporter structure (Figure 4B). However, superposition of only α6 and α7 reveals a similar backbone

trace (RMSD 1.5 Å over 54 $C_\alpha$; Figure 4C). From this analysis, the loop connecting α5–α6 seems largely responsible for the conformational change observed in $AfCorA_{1-263}$. We refer to this loop as the 'CorA elbow' (Figure 4A–C).

Beyond considering $AfCorA_{1-263}$ a crystallization artifact, a model for $TmCorA_{1-263}$ was constructed based on the $AfCorA_{1-263}$ structure and positioned onto the full-length transporter. Guided by steric considerations alone (i.e. clashes), only one model for the presumed 'open state' appears feasible (Figure 5B). Strikingly, α6 would rotate ~105° around α7, so we refer to α6 as the 'swivel helix'. A closer examination of $AfCorA_{1-263}$ reveals that α6 is slightly rotated, and becomes unwound towards the membrane proximal region (Figure 4C). Thus, the swivel helix itself contains a 'swing'. When viewed end on, transition to the open state model can be described as the counterclockwise rotation of α6 around α7 with a concurrent ~180° clockwise swing of the membrane proximal portion of α6; this is coupled to a ~30° opening of the CorA elbow (Figure 5A and B). The hammer domains presumably slide along the periphery of α7 during these motions. It is important to note that the loop connecting α6–α7 appears to remain rigid (Figure 4C). Therefore, movements of the swivel helix should impart significant torque along α7.

### *A two-state model*

In addition to the $AfCorA_{1-263}$ crystal structure, various lines of evidence support the presented open state model. There is significant conservation within the α5–α6 region and a glycine or proline residue is highly conserved in the CorA elbow (Figure 1C). Moreover, the elbow also appears to be a dynamic structural element. In $TmCorA_{SGC}$ and $TmCorA_{1-351}$, this is suggested by elevated crystallographic B-factors and poor electron density. As the elbow was untraceable in a 1.85 Å soluble domain structure of $TmCorA_{SGC-266}$ (PDB 2BBH; space group $P4_12_12$; Lunin *et al*, 2006), this trend is not resolution dependent. A report that *Escherichia coli* CorA could only be isolated in a stable form upon the addition of $Mg^{2+}$ (Eshaghi *et al*, 2005) supports our view that the CorA elbow may function (like a spring) in connection with the metal site occupancy at the divalent cation sensor. Although the cations located at the protomer interface (Figure 3B) may clearly play a role in stabilizing TmCorA (Supplementary Figures 2 and 3), they are not required to maintain its pentameric state (Supplementary Figure 4). These results are consistent with the notion that CorA gating responds to low intracellular substrate concentrations.

We sought evidence of a conformation change in TmCorA based on the observation that the N-terminal flap, residues

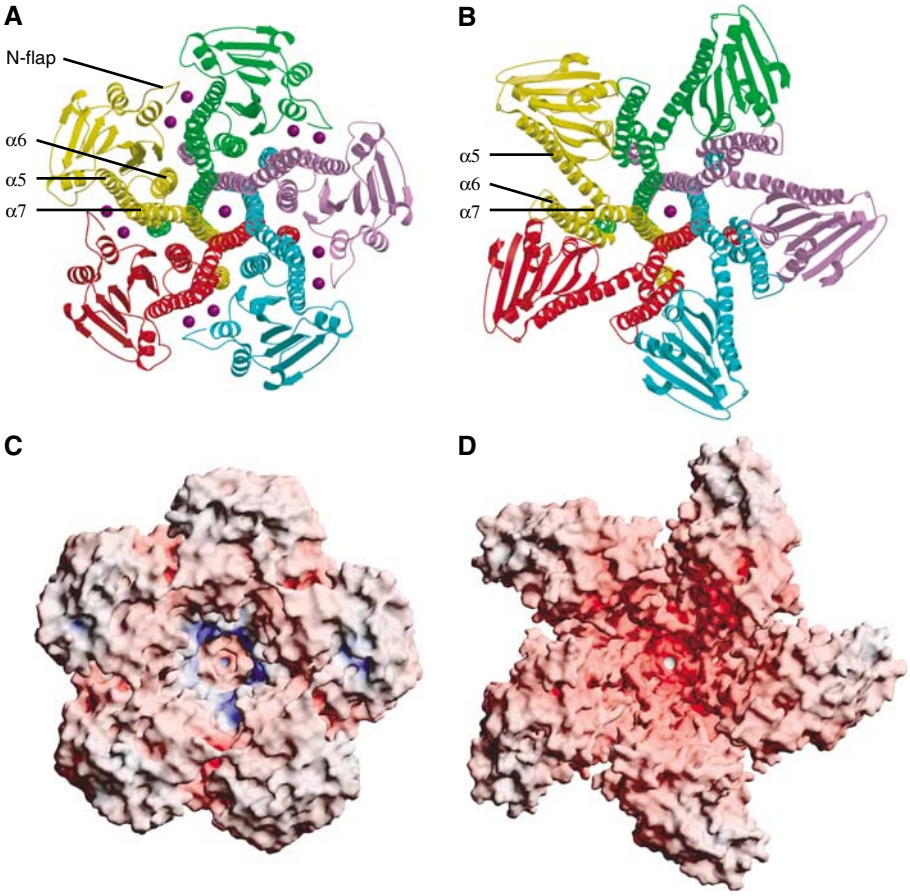


**Figure 5** Closed and open state models. (**A**) The crystal structure of $TmCorA_{1-351}$. A view looking into the funnel domain from the cytoplasmic side. Protomers are individually colored and purple spheres represent bound $Ca^{2+}$ ions. α5, α6, α7, and the N-terminal flap (i.e., N-flap) are indicated. (**B**) A model for the CorA open state. The N-terminal flap residues were removed and $Ca^{2+}$ ions in the pore are shown for reference only. (**C**) Electrostatic surface potential of the CorA closed state (same view as part A). Red – acidic regions; blue – basic regions. Bound $Ca^{2+}$ ions were omitted from the calculation. The basic character is largely established by the 'neutralizing residues' contributed from α6. Note, the acidic interface between protomers houses the divalent cation sensor. (**D**) Electrostatic surface potential of the CorA open state model (same view as part B). Red – acidic regions; blue – basic regions. $Ca^{2+}$ ions were omitted from the calculation.

1–25, would clash in our open state model if maintained in its 'closed state' conformation (Figure 5A and B). As portions of the N-terminal flap are 'invisible' in all available crystal structures, and the well-characterized StCorA and MjCorA proteins lack this sequence (Figure 1C), we reasoned that this region may become disordered (and therefore susceptible to exogenous protease) in the open state of the transporter. Indeed, incubation of TmCorA in the presence or absence of $Mg^{2+}$ reveals differential susceptibility to trypsin. Surprisingly, relative to 4°C, incubation at 37°C protects TmCorA from digestion. This result is more obvious with extended incubation times, where one finds dramatic protection of TmCorA in the presence of $Mg^{2+}$ at 4°C (Figure 6A and B). After ruling out the possibility of cold denaturation (Supplementary Figures 2, 3, and 4), the most straightforward interpretation is that TmCorA becomes 'resistant' to trypsin in a divalent cation-dependent manner. Thus, the trypsin-protected conformation presumably reflects the closed state observed in the $TmCorA_{1-351}$ crystal structure (Figures 1A, 5A, and Supplementary Figure 3). The differential protease susceptibility of TmCorA is suggestive of a significant conformational change, and the degradation pattern is consistent with two defined conformational states (Figure 6A and B).

A thermodynamic trap may explain the increased susceptibility of TmCorA to trypsin at 4°C. Based on our open state model, we assume that the lower temperature slows the return of the CorA elbow and swivel helix to their closed state positions (Figure 5A and B); and consequently, increase the susceptibility of TmCorA to trypsin. Relative to the EDTA conditions at 37°C, that TmCorA is susceptible even in the presence of high $Mg^{2+}$ concentrations is somewhat unexpected (Figure 6A and B). Although the activation of trypsin by certain divalent cations needs to be considered (Green and Neurath, 1953), this result might suggest that an intermittent opening of the transporter occurs under conditions in which $Mg^{2+}$ concentrations are not physiologically limiting. Nonetheless, our data and model would predict that opening and closing of CorA occurs in a concerted manner involving all protomers.

### *Probing a global divalent cation sensor*

Employing the established protease protection assay, titration experiments support the notion that CorA contains a divalent

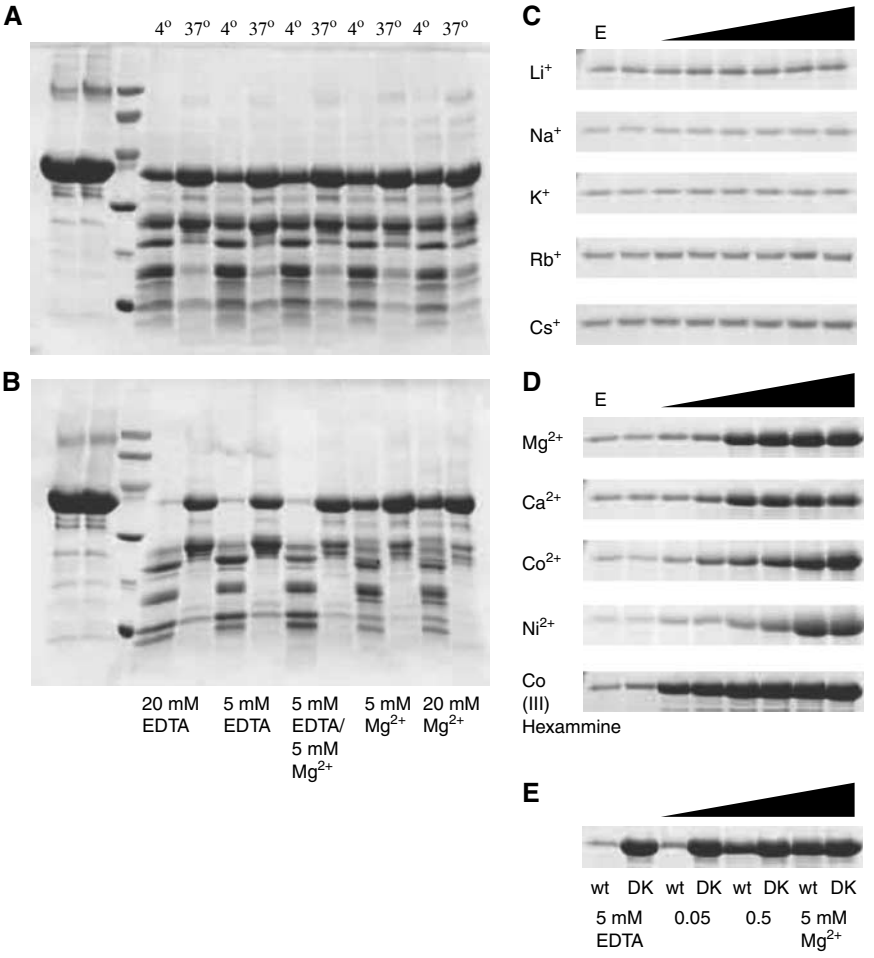


**Figure 6** Protease susceptibility assay. (**A, B**) Trypsin susceptibility of $TmCorA_{1-351}$ after (A) 1 h and (B) 15 h. Reactions were performed as described in Materials and methods. Control samples provided in the first two lanes are representative of the different experimental conditions. Third lane – molecular weight ladder: 94, 67, 43, 30, 20, and 14 kDa, respectively. (**C, D**) Based on the results of (A, B), trypsin susceptibility was investigated at 4°C with 15 h incubations. 5 mM EDTA control. Cation concentrations from left to right are: 0, 0.05, 0.1, 0.5, 1, 2.5, and 5 mM. (**E**) The experiments described in (C, D) were also used to compare the wild-type (wt) $TmCorA_{1-351}$ protein to the Asp253-to-Lys253 mutant (DK). Reaction conditions are indicated.

 

cation sensor. Specifically, the monovalent cations: $Li^+$, $Na^+$, $K^+$, $Rb^+$, and $Cs^+$ offered TmCorA no protection at the concentrations tested (Figure 6C). With respect to $Mg^{2+}$, concentrations that afford TmCorA protection are centered within a physiologically meaningful range, that is, $\sim$0.5 mM (Figure 6D; Hartwig, 2001; Maguire and Cowan, 2002; Kolisek *et al*, 2003; Froschauer *et al*, 2004; Cromie *et al*, 2006). This result suggests that the divalent cation sensor functions as a molecular switch, and also acts as a global $Mg^{2+}$ homeostatic meter. The minimum protection threshold for TmCorA is $\sim$50 μM $Mg^{2+}$ (Figure 6D); remarkably, this set point lies just below the extracellular concentrations required to activate the PhoP/PhoQ two-component system to transcribe the *mgtA* and *mgtB* $Mg^{2+}$ transporter genes (Garcia Vescovi *et al*, 1996; Cromie *et al*, 2006). Concentrations that offer TmCorA no protection, that is, $<$50 μM $Mg^{2+}$ (Figure 6D), are the exact conditions that derepress *mgtA* translation (Cromie *et al*, 2006). Therefore, together with previous work (Garcia Vescovi *et al*, 1996; Cromie *et al*, 2006), this study begins to reveal the hierarchy and coordination of prokaryotic $Mg^{2+}$ homeostasis at the molecular level. It is tempting to speculate that an analogous regulatory mechanism exists within the eukaryotic CorA orthologues (Kolisek *et al*, 2003).

The substrates $Co^{2+}$ and $Ni^{2+}$ also offer TmCorA protection, but at relatively high concentrations (i.e. $\sim$50 μM; Figure 6D). In order to appreciate the relevance to CorA biology, one must consider the extremely low intracellular concentrations of these cations (Outten and O'Halloran, 2001), and also the freely available intracellular concentrations of the cation in question. For example, there is $<$1 free $Zn^{2+}$ ion per cell (Outten and O'Halloran, 2001); the corresponding numbers for $Ca^{2+}$ are $\sim$30, $Mg^{2+}$ $\sim$90 000, and for $Na^+$ and $K^+$ $>2\times10^6$ (Maguire and Cowan, 2002). This implies that the CorA divalent cation sensor is '$Mg^{2+}$-specific' under physiological settings.

Given the architecture of the divalent cation sensor (Figure 3B), one unanticipated finding is that cobalt(III)-hexammine offers TmCorA strong protection from trypsin proteolysis (Figure 6D). Cobalt(III)hexammine has ammine moieties tightly bound to cobalt, is a potent inhibitor of CorA transport, and is nearly the size of a hydrated $Mg^{2+}$ ion (Kucharski *et al*, 2000; Kolisek *et al*, 2003). When considering that neither $Mg^{2+}$, $Co^{2+}$, $Ni^{2+}$, or $Ca^{2+}$ provided such protection (Figure 6D), this result could be consistent with the proposal that cobalt(III)hexammine and other hydrated cations occupy at least one position within the CorA pore (Figure 2B). As such, this finding might suggest that substrate dehydration is a requisite and early event in the CorA translocation cycle.

Finally, we created an Asp253-to-Lys253 TmCorA mutant (DK). A lysine side chain should mimic a bound cation and lead to the formation of a salt bridge with Asp89′ (Figure 3B); thus, we predicted that the DK mutant would be resistant to trypsin in a divalent cation-independent manner. Indeed, even in the complete absence of $Mg^{2+}$, the DK mutant is markedly protected from trypsin digestion (Figure 6E). We also find that the DK mutant is considerably more stable than the wild-type protein (Supplementary Figure 2); and, in contrast to the wild-type protein (Payandeh and Pai, 2006), the DK mutant crystallizes readily in the absence of added divalent cations (data not shown). Taken together, these results support the notion of a conformational change in CorA, and implicate the involvement of the divalent cation sensor.

## Discussion

### *CorA points of interest*

Lunin *et al*, have proposed that substrate specificity in CorA is achieved by four consecutive properties of the transporter. First, the highly conserved periplasmic or extracellular MPEL sequences constitute part of the selectivity filter. Second, the Asn314 side chains of the GMN motif interact initially with hydrated substrates, and subsequently dehydrate them (at least partially). Third, the polar lining of the pore entrance compensates for the energetic cost of $Mg^{2+}$ dehydration. Fourth, Leu294 is critical for achieving specificity by imposing a constriction that would allow transport of the uniquely small $Mg^{2+}$ ion, a feature they suggest will gate the transporter (Lunin *et al*, 2006).

Several aspects of the above proposal are not supported by our data. For instance, our maps indicate that the MPEL sequences lie almost perpendicular to the pore entrance (Figure 2A); this position does not seem particularly conducive to being part of the selectivity filter. Furthermore, $TmCorA_{SGC}$ was solved in the presence of $Mg^{2+}$ (Lunin *et al*, 2006), conditions that one would expect to order the selectivity filter (Zhou and MacKinnon, 2003); however, the MPEL loops in $TmCorA_{SGC}$ could not be modeled (Lunin *et al*, 2006). Moreover, the well-characterized MjCorA is extremely deviant within the MPEL motif, conserving only the proline residue (Figure 1C). Thus, we assign this loop a role in linking potential movements of TM2 to the CorA pore, but leave open the possibility that it may have other functional and/or structural roles (e.g. increasing the local cation concentration, or being involved in protein folding).

Lunin *et al* (2006) suggest that Asn314 plays a critical role in dehydrating incoming $Mg^{2+}$ ions, and that this is a key basis for selectivity in CorA. While we assume that Asn314 plays an important role in 'screening' potential substrates, these side chains have moved up to 3 Å in our structure relative to $TmCorA_{SGC}$ (Figure 2C). This seems more consistent with a role in gating (Dutzler *et al*, 2003). In fact, the entire GMN motif backbone has shifted in our structure, as if to be pulled 'towards' TM2 (Figure 2C and D). These displacements might be more representative of the open state; they may also illustrate consequences associated with even minor movements of TM2 (Figure 2D) and the MPEL loop. Finally, our data indicate that a hydrated cation exists within the pore beyond Asn314 (Figure 2B).

### *A proposal for specificity and transport in CorA*

What is the hydration status of $Mg^{2+}$ within the CorA pore? It is unlikely that a completely dehydrated $Mg^{2+}$ ion will travel the distance in CorA as, beyond energetic considerations, this would produce a large discrepancy between the pore dimensions and the ionic radius of $Mg^{2+}$. It also seems unlikely that the Leu294 gate will function as the selectivity filter in CorA. For one, Leu294 sits at the intracellular lipid–aqueous interface (Figure 2A and D); moreover, the pore constriction at Leu294 is only $\sim$2.5 Å, making selection between the ionic forms of $Mg^{2+}$ and the non-CorA substrates $Ca^{2+}$, $Mn^{2+}$, $Zn^{2+}$, and $Fe^{2+}$ (Snavely *et al*, 1989; Papp and Maguire, 2004) nearly impossible.

As $Mg^{2+}$ has the smallest ionic radius and the largest hydrated radius among the common biological cations (Maguire and Cowan, 2002), we anticipate that CorA will exploit these properties to achieve substrate specificity and transport. We propose that the CorA pore may contain multiple hydrated metal 'binding' sites intervened by discrete hydrophobic constrictions (Figure 2B). While reducing the overall energetic cost of transporting a completely dehydrated $Mg^{2+}$ ion, this scenario might afford CorA the opportunity to maximize specificity by sensing both the hydrated and ionic radii of its substrates. We suggest a 'linked-beads' type of translocation model, where cations move in discrete and concerted steps along the translocation path. Incoming substrates should force existing metals along the pore; and an intracellular electrostatic sink will help to draw cations out of it. This mechanism could permit the rapid initiation and cessation of transport, conceivably trapping potential substrates during transit (Figure 2A–D). While consistent with a large body of evidence for other proteins (Zhou *et al*, 2001; Gouaux and Mackinnon, 2005; Lobet and Dutzler, 2006; Shi *et al*, 2006), this proposal can accommodate the high flux rates measured in various members of the CorA superfamily (Snavely *et al*, 1989; Liu *et al*, 2002; Kolisek *et al*, 2003).

CorA is known to transport $Co^{2+}$ and $Ni^{2+}$, which have comparable ionic radii and share a similar hexacoordinate preference with $Mg^{2+}$ (Harding, 2004); cobalt(III)hexammine, a potent inhibitor of CorA transport, is nearly the same size as a hydrated $Mg^{2+}$ ion. These considerations imply that the small ionic radii of $Mg^{2+}$, $Co^{2+}$, and $Ni^{2+}$ are important for their transport, and that CorA interacts with hydrated substrates, at least initially. In addition to sensing size, the commonalities between $Mg^{2+}$, $Co^{2+}$, $Ni^{2+}$, and cobalt(III)hexammine also suggest that CorA might identify substrates through preferences in their coordination geometry. However, as most cations are quite sparse in biological settings, perhaps CorA may only need to select between $Na^{+}$, $K^{+}$, $Ca^{2+}$, and $Mg^{2+}$. An analogous suggestion has been made for the Alr1 proteins (MacDiarmid and Gardner, 1998) and the ClC superfamily (Gouaux and Mackinnon, 2005; Lobet and Dutzler, 2006).

We believe that Site A represents a principal component of the selectivity filter in CorA (Figure 2B). We first consider $Ca^{2+}$, assigned in our structure, and will extend these considerations to $Na^{+}$ and $K^{+}$. Although $Ca^{2+}$ is neither a substrate nor a good inhibitor of CorA (Snavely *et al*, 1989), it still seems capable of proceeding beyond Asn314 and appears hydrated at Site A (Figure 2B). It is notable that the hydrated radii of $Na^{+}$, $K^{+}$, and $Ca^{2+}$ are similar, and $\sim$1.5–2 Å smaller than that of $Mg^{2+}$ (Maguire and Cowan, 2002). Thus, it is possible that ions with a small hydration shell might not interact with CorA strongly enough to be transported, and may simply diffuse away. As a very large hydration shell would clash with the pore walls, steric restriction should occlude any larger species (Kucharski *et al*, 2000). Hence, the CorA pore is probably optimized for hydrated substrates that fit 'just right' at Site A to promote their transit past the hydrophobic belt (Figure 2B). The cation hexammine inhibitors (Kucharski *et al*, 2000) might then plug the pore at Site A because they cannot undergo the necessary 'dehydration' at the Thr305/Met302 hydrophobic belt. Compared to inhibition at Asn314 (Lunin *et al*, 2006), this model may explain why cobalt(III)hexammine has a higher affinity for CorA than does $Mg^{2+}$ itself (Kucharski *et al*, 2000).

Additional factors likely play a role in the selectivity, regulation, and transport cycle of CorA. For example, a second dehydration event at the hydrophobic girdle could impose further specificity. Also, movements impinged onto TM2 could regulate the status of the Asn314 gate through the MPEL loop. This would promote a reloading of substrates into Site A and the translocation of metals along the pore.

### *The CorA transport cycle*

If we assume a two-state model (Figures 5 and 7), there are at least three consequences to consider in the closed-to-open state transition of TmCorA. First, movement of the swivel helix will impart a dramatic acidic charge character at the intracellular end of the pore (Figure 5D). This should provide critical energetic contributions to promote transport and draw $Mg^{2+}$ through the pore. Second, given the rigid nature of the loop connecting the swivel helix to α7 (Figure 4C), considerable torque will be generated along α7. In fact, the open state model requires a 'translation' of α7 by $\sim$1/3 of a helical turn. This twist would be an effective mechanism to impose a gating force onto Leu294, a residue $\sim$55 Å away from the α6–α7 loop. Third, the acidic ring on the funnel domain exterior (Figure 3A) must undergo significant rearrangement during these movements, which is likely to have an impact upon the basic ring that sits atop TM2 (Figure 3A). We predict that this will influence the relative position and/or orientation of TM2 within the membrane bilayer, although perhaps only by a small amount (Figure 2D). In sum, we propose that the outcome of these conformational changes will simultaneously prime the CorA funnel domain interior, the Leu294 gate, and the Asn314 periplasmic gate for $Mg^{2+}$ transport (Figure 7).

What are the components leading to opening of the transporter? The loss of cation coordination at the divalent cation sensor should set in motion events leading to the open state. As the charge character of the protomer–protomer interface is quite acidic (Figure 5C), loss of cations would result in significant charge repulsion. Perhaps this perturbation allows the CorA elbow to withdraw the swivel helix from its closed state position on route to the open state.

What are the components leading to closure of the transporter? Torque generated on α7 should be one force driving a return to the closed state. Recoiling of the α6 'swing' and the CorA elbow could be others. Steric restriction on the hammer domain will promote this process, and the domain-swapped arrangement observed in the $AfCorA_{1-263}$ crystal structure (Figure 4A and B) suggests that the hammer domain has an inherent affinity for the closed state. Finally, a local influx of divalent cations, in accordance with the open state, will increase the probability of occupying the divalent cation sensor and help to shut down transport.

### *Perspectives*

Beyond the nature of its pore, perhaps one of the most intriguing features about CorA is its channel-like architecture. Although obviously unique, CorA seems strangely reminiscent of the $K^{+}$-type channels (Zhou *et al*, 2001; Zhou and MacKinnon, 2003; Shi *et al*, 2006); and we begin to draw

 

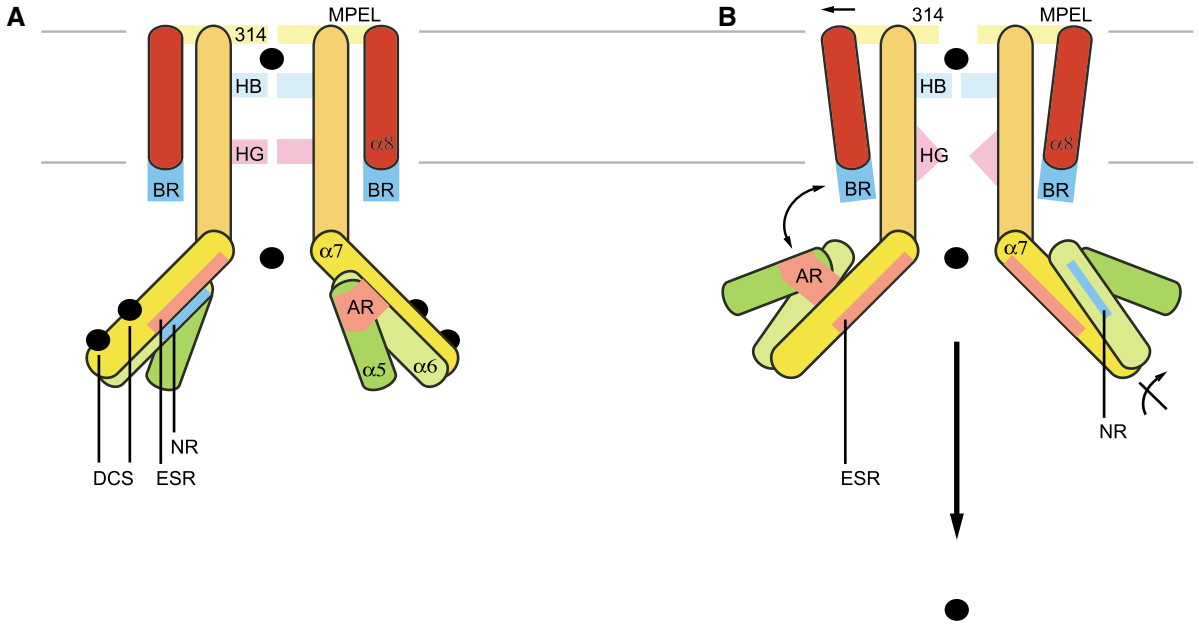


**Figure 7** A schematic model of the CorA translocation cycle. (**A**) The CorA closed state. This conformation presumably represents that observed in the $TmCorA_{1-351}$ crystal structure and the condition in which there is an adequate or high intracellular $Mg^{2+}$ concentration. The color coding is consistent with Figure 1C and major structural features are indicated as follows: MPEL – MPEL loop; 314 – Asn314 gate; HB – hydrophobic belt (residues Met302 and Thr305); HG – hydrophobic girdle (residues Met291 and Leu294); BR – basic ring (residues Lys346-Lys349); AR – acidic ring; NR – neutralizing residues (α6); ESR – electrostatic sink residues (α7); DCS – divalent cation sensor; black spheres – $Mg^{2+}$ ions. Only two CorA protomers are shown and, except for α5, the hammer domain has been omitted for clarity. (**B**) The CorA open state. Implications of the conformational changes in CorA associated with an inadequate or low intracellular $Mg^{2+}$ concentration. With the loss of $Mg^{2+}$ coordination at the DCS, charge repulsion between protomers and the dynamic CorA elbow region have been implicated in bringing about movements of α6 (the swivel helix), α5, and the hammer domain. This should impart a force onto the Leu294 gate (at the HG) through a twisting of α7. A rearrangement of the AR should impinge onto the BR and effect the position and/or orientation of TM2 (i.e. α8) within the membrane bilayer; this is predicted to open the Asn314 gate through movements of the MPEL loop. As the NR on α6 have been 'withdrawn', the ESR on α7 will create an acidic environment within the funnel domain interior that will promote ion transport. Factors mentioned in the main text will return CorA to the closed state position shown in (A). Beyond regulating the transport status of CorA, the DCS (in effect) also acts as an intracellular $Mg^{2+}$ sensor.

many parallels with the acetylcholine receptor (Doyle, 2004; Unwin, 2005). Under normal conditions, however, CorA is strictly a 'transporter', functioning to move $Mg^{2+}$ against its concentration gradient. Yet, CorA and CorA homologues also function as effluxers; and some of these proteins assume channel-like properties. Thus, the line between an ion channel and an ion transporter has become blurred. CorA, however, does not set this precedent. For example, the ClC superfamily of chloride channels and transporters share nearly identical structures (Dutzler *et al*, 2003; Lobet and Dutzler, 2006), and the projection structure of the human copper transporter CTR1 has revealed a homo-oligomeric channel-like architecture (Aller and Unger, 2006).

Metals found along the pore in $TmCorA_{1-351}$ have provided clues to the principles of substrate specificity and transport. A hydrophobic gate and a hydrated metal stabilized within the TM region are emerging as channel-specific and cation-specific themes (Zhou *et al*, 2001; Doyle, 2004; Shi *et al*, 2006). This work has also unveiled a physiologically tuned divalent cation sensor within TmCorA. Thus, CorA has an intrinsic allosteric regulatory switch that may control $Mg^{2+}$ homeostasis at the cellular level. Based on crystallographic, biochemical, and biophysical data, our model of the open state presents a cohesive structural framework for the translocation cycle of CorA. Hopefully, this will provide a foundation for further study of structure–function relationships within the ubiquitous CorA superfamily.

## Materials and methods

### *Crystallization and data collection*

Details on protein purification and crystallization have been reported elsewhere (Payandeh and Pai, 2006). The DK mutant was produced using the QuikChange protocol (Stratagene) and all constructs were confirmed by DNA sequencing. The final protein buffers were 20 mM Tris pH 8.0, 100 mM NaCl, 1 mM TCEP; with or without 0.026% *n*-dodecyl-β-D-maltoside (Anatrace). Besides $CaCl_2$, no other divalent cations were added during the purification or crystallization of $TmCorA_{1-351}$.

$TmCorA_{1-351}$ (15 mg/ml; 0.026% *n*-dodecyl-β-D-maltoside) was crystallized in the space group *C*2 by vapor-diffusion over 20% PEG 400, 0.2 M $CaCl_2$, 0.1 M HEPES pH 7.0. Native and SeMet-$AfCorA_{1-263}$ (40 mg/ml) were crystallized in the space group $P6_122$ over 1.3 M ammonium sulfate, 10 mM $CoCl_2$, 0.1 M HEPES pH 7.4. X-ray data were collected at the NSLS X8C beamline as described (Payandeh and Pai, 2006). X-ray data were processed using DENZO/SCALEPACK (Otwinowski and Minor, 1997) and the CCP4 suite (CCP4, 1994) (Supplementary Table 1).

### *Structure determination and refinement*

See Supplementary Materials and methods. Structure factors and coordinates for $AfCorA_{1-263}$ and $TmCorA_{1-351}$ have been deposited in the PDB (www.rcsb.org) under the accession codes 2HN1 and 2HN2, respectively.

### *Alignments and the open state model*

ClustalW (Thompson *et al*, 1994) was used for Figure 1C. LSQMAN (Kleywegt, 1996) was used for all structural alignments. A model of $TmCorA_{1-263}$ was built using LSQMAN to align residues 17–201 and residues 205–263 of $TmCorA_{1-351}$ over equivalent portions of $AfCorA_{1-263}$ as shown in Figure 4C. The CorA elbow was then

rebuilt manually in O (Jones *et al*, 1991), and the $TmCorA_{1-263}$ model was docked onto the full-length $TmCorA_{1-351}$ structure using O.

***Molecular figures and electrostatic surface calculations***
Structural figures were prepared using MOLSCRIPT (Kraulis, 1991) and RASTER3D (Merritt and Murphy, 1994). After removal of cations, the electrostatic surfaces shown in Figures 3A, 5C and D were generated using SPOCK (Christopher, 1998).

***Protease susceptibility assay***
For 50 µl reaction volumes, stock solutions were prepared to produce the final concentrations desired upon dilution: 38.75 µl of protein (2.58 mg/ml), 1.25 µl of trypsin (10 mg/ml; Sigma), and 10 µl of 0–100 mM of 'substrate'. Reaction solutions were mixed and equilibrated at 4°C for 20 min. Trypsin was then added, and reactions were incubated at 4 or 37°C for the specified times. After adding 50 µl of SDS–PAGE sample buffer, samples were boiled and run immediately on 15% SDS–PAGE gels. To rule out the possibility of trypsin inhibition, controls were performed on a test protein over the full range of conditions.

***Circular dichroism and gel filtration***
See Supplementary Materials and methods.

***Supplementary data***
Supplementary data are available at *The EMBO Journal* Online.

***Note added in proof***
While this manuscript was in press, two related reports have appeared. Eshaghi *et al* (2006, *Science* **313:** 354–357) have described the crystal structure of TmCorA at 2.9 Å resolution, which is largely the same as the $TmCorA_{1-351}$ structure presented here. Wang *et al* (2006, *JBC* PMID: 16835234) have performed electron microscopy analysis on a soluble portion of *E. coli* CorA. Although these authors describe $EcCorA_{1-223}$ as a periplasmic tetramer, their electron density envelope seems highly reminiscent of our CorA 'open state' model.

## Acknowledgements

JP dedicates this work to the memory of his friend Lee Julott, and appreciates the continued support of Emily Cowan, Wing Lau, Wanda Gillon, and Dr Masahiro Fujihashi. We acknowledge the membrane protein clones, selected by JP, initially provided by Drs Aled Edwards and Alexei Savchenko. We thank the staff at the X8C beamline for their help during data collection. A joint grant from the Canadian Institutes of Health Research and National Sciences and Engineering Research Council of Canada enabled the use of X8C at the National Synchrotron Light Source, Brookhaven National Laboratory. This work was supported by the Canada Research Chairs Program and the National Sciences and Engineering Research Council of Canada (EFP).

## References

Aller SG, Unger VM (2006) Projection structure of the human copper transporter CTR1 at 6-Å resolution reveals a compact trimer with a novel channel-like architecture. *Proc Natl Acad Sci USA* **103:** 3627–3632

Bui DM, Gregan J, Jarosch E, Ragnini A, Schweyen RJ (1999) The bacterial magnesium transporter CorA can functionally substitute for its putative homologue Mrs2p in the yeast inner mitochondrial membrane. *J Biol Chem* **274:** 20438–20443

CCP4 (1994) The CCP4 suite: programs for protein crystallography. *Acta Crystallogr D Biol Crystallogr* **50:** 760–763

Christopher JA (1998) *SPOCK: The Structural Properties Observation and Calculation Kit (Program Manual). The Center for Macromolecular Design*. Texas A&M University, College Station, TX

Cromie MJ, Shi Y, Latifi T, Groisman EA (2006) An RNA sensor for intracellular $Mg^{2+}$. *Cell* **125:** 71–84

Doyle DA (2004) Structural changes during ion channel gating. *Trends Neurosci* **27:** 298–302

Dutzler R, Campbell EB, MacKinnon R (2003) Gating the selectivity filter in ClC chloride channels. *Science* **300:** 108–112

Eshaghi S, Hedren M, Nasser MI, Hammarberg T, Thornell A, Nordlund P (2005) An efficient strategy for high-throughput expression screening of recombinant integral membrane proteins. *Protein Sci* **14:** 676–683

Froschauer EM, Kolisek M, Dieterich F, Schweigel M, Schweyen RJ (2004) Fluorescence measurements of free [$Mg^{2+}$] by use of magfura 2 in *Salmonella enterica*. *FEMS Microbiol Lett* **237:** 49–55

Garcia Vescovi E, Soncini FC, Groisman EA (1996) $Mg^{2+}$ as an extracellular signal: environmental regulation of Salmonella virulence. *Cell* **84:** 165–174

Gouaux E, Mackinnon R (2005) Principles of selective ion transport in channels and pumps. *Science* **310:** 1461–1465

Green NM, Neurath H (1953) The effects of divalent cations on trypsin. *J Biol Chem* **204:** 379–390

Harding MM (2004) The architecture of metal coordination groups in proteins. *Acta Crystallogr D Biol Crystallogr* **60:** 849–859

Hartwig A (2001) Role of magnesium in genomic stability. *Mutat Res* **475:** 113–121

Jones TA, Zou JY, Cowan SW, Kjeldgaard M (1991) Improved methods for building protein models in electron density maps and the location of errors in these models. *Acta Crystallogr A* **47:** 110–119

Kehres DG, Maguire ME (2002) Structure, properties and regulation of magnesium transport proteins. *Biometals* **15:** 261–270

Kleywegt GJ (1996) Use of non-crystallographic symmetry in protein structure refinement. *Acta Crystallogr D Biol Crystallogr* **52:** 842–857

Kloda A, Ghazi A, Martinac B (2006) C-terminal charged cluster of MscL, RKKEE, functions as a pH sensor. *Biophys J* **90:** 1992–1998

Knoop V, Groth-Malonek M, Gebert M, Eifler K, Weyand K (2005) Transport of magnesium and other divalent cations: evolution of the 2-TM-GxN proteins in the MIT superfamily. *Mol Genet Genomics* **274:** 205–216

Kolisek M, Zsurka G, Samaj J, Weghuber J, Schweyen RJ, Schweigel M (2003) Mrs2p is an essential component of the major electrophoretic $Mg^{2+}$ influx system in mitochondria. *EMBO J* **22:** 1235–1244

Kraulis PJ (1991) MOLSCRIPT: a program to produce both detailed and schematic plots of protein structures. *J Appl Crystallogr* **24:** 946–950

Kucharski LM, Lubbe WJ, Maguire ME (2000) Cation hexaammines are selective and potent inhibitors of the CorA magnesium transport system. *J Biol Chem* **275:** 16767–16773

Li L, Tutone AF, Drummond RS, Gardner RC, Luan S (2001) A novel family of magnesium transport genes in Arabidopsis. *Plant Cell* **13:** 2761–2775

Liu GJ, Martin DK, Gardner RC, Ryan PR (2002) Large $Mg^{2+}$-dependent currents are associated with the increased expression of ALR1 in *Saccharomyces cerevisiae*. *FEMS Microbiol Lett* **213:** 231–237

Lobet S, Dutzler R (2006) Ion-binding properties of the ClC chloride selectivity filter. *EMBO J* **25:** 24–33

Lunin VV, Dobrovetsky E, Khutoreskaya G, Zhang R, Joachimiak A, Doyle DA, Bochkarev A, Maguire ME, Edwards AM, Koth CM (2006) Crystal structure of the CorA $Mg^{2+}$ transporter. *Nature* **440:** 833–837

MacDiarmid CW, Gardner RC (1998) Overexpression of the *Saccharomyces cerevisiae* magnesium transport system confers resistance to aluminum ion. *J Biol Chem* **273:** 1727–1732

Maguire ME, Cowan JA (2002) Magnesium chemistry and biochemistry. *Biometals* **15:** 203–210

Merritt EA, Murphy ME (1994) Raster3D Version 2.0. A program for photorealistic molecular graphics. *Acta Crystallogr D Biol Crystallogr* **50:** 869–873

Otwinowski Z, Minor W (1997) Processing of X-ray diffraction data collected in oscillation mode. In: Carter CWJ, Sweet RM (eds) *Methods in Enzymology*, pp 307–326. New York: Academic Press

Outten CE, O'Halloran TV (2001) Femtomolar sensitivity of metalloregulatory proteins controlling zinc homeostasis. *Science* **292:** 2488–2492

Papp KM, Maguire ME (2004) The CorA $Mg^{2+}$ transporter does not transport $Fe^{2+}$. *J Bacteriol* **186:** 7653–7658

 

Payandeh J, Pai EF (2006) Crystallization and preliminary X-ray diffraction analysis of the magnesium transporter CorA. *Acta Crystallograph Sect F Struct Biol Cryst Commun* **62:** 148–152

Shi N, Ye S, Alam A, Chen L, Jiang Y (2006) Atomic structure of a $Na^+$- and $K^+$-conducting channel. *Nature* **440:** 570–574

Smith RL, Szegedy MA, Kucharski LM, Walker C, Wiet RM, Redpath A, Kaczmarek MT, Maguire ME (1998) The CorA $Mg^{2+}$ transport protein of *Salmonella typhimurium*. Mutagenesis of conserved residues in the third membrane domain identifies a $Mg^{2+}$ pore. *J Biol Chem* **273:** 28663–28669

Snavely MD, Florer JB, Miller CG, Maguire ME (1989) Magnesium transport in *Salmonella typhimurium*: $^{28}Mg^{2+}$ transport by the CorA, MgtA, and MgtB systems. *J Bacteriol* **171:** 4761–4766

Thompson JD, Higgins DG, Gibson TJ (1994) CLUSTAL W: improving the sensitivity of progressive multiple sequence alignment through sequence weighting, position-specific gap penalties and weight matrix choice. *Nucleic Acids Res* **22:** 4673–4680

Unwin N (2005) Refined structure of the nicotinic acetylcholine receptor at 4 Å resolution. *J Mol Biol* **346:** 967–989

von Heijne G (1989) Control of topology and mode of assembly of a polytopic membrane protein by positively charged residues. *Nature* **341:** 456–458

Worlock AJ, Smith RL (2002) ZntB is a novel $Zn^{2+}$ transporter in *Salmonella enterica* serovar Typhimurium. *J Bacteriol* **184:** 4369–4373

Zhou Y, MacKinnon R (2003) The occupancy of ions in the $K^+$ selectivity filter: charge balance and coupling of ion binding to a protein conformational change underlie high conduction rates. *J Mol Biol* **333:** 965–975

Zhou Y, Morais-Cabral JH, Kaufman A, MacKinnon R (2001) Chemistry of ion coordination and hydration revealed by a $K^+$ channel–Fab complex at 2.0 Å resolution. *Nature* **414:** 43–48

Zsurka G, Gregan J, Schweyen RJ (2001) The human mitochondrial Mrs2 protein functionally substitutes for its yeast homologue, a candidate magnesium transporter. *Genomics* **72:** 158–168